

## Cluster interactions and physical properties of Al-transition-metal alloys

A. E. Carlsson

*Department of Physics, Washington University, St. Louis, Missouri 63130*

(Received 12 May 1988; revised manuscript received 1 November 1988)

Ising-like interaction parameters are calculated for alloys of Al with the  $3d$  and  $4d$  transition metals. The interactions are obtained by matching to calculated total energies for supercell compounds on an underlying fcc lattice. The dependence of the parameters on the transition-metal  $d$ -band filling displays pronounced oscillations, which are interpreted in terms of the width and shape of the electronic density of states. The interactions are used to provide the first unified *ab initio* description of a wide variety of phenomena in these alloys. Results for heats of solid solution in transition-metal-rich alloys are in good agreement with experimental values for fcc and hcp phases. Observed chemical trends in solid solubilities, including the values in Al-Mn, are confirmed and explained. Effective pair interactions for describing short-range order are in fairly good agreement with empirical values obtained from short-range-order data and other observations.

### I. INTRODUCTION

Alloys of Al with transition metals have for decades received considerable attention in the materials-science community. The primary motivation for this has been the desirable technological properties<sup>1</sup> of many of these alloys, including a combination of light weight and high strength if the alloy is appropriately treated. The Al-Cu, Al-Ti, and Al-Ni systems are prime examples of these properties. More recently, the discovery<sup>2</sup> of quasicrystalline phases of Al-transition-metal alloys has attracted interest from an even broader audience. To explain the remarkable properties of these alloys, it is necessary to perform calculations at an atomistic level, which often require a description of the bonding energetics in terms of interatomic potentials, or Ising-like interaction parameters. The purpose of this paper is to present the values of such interaction parameters, to explain the origin of their variation with the number of transition-metal  $d$  electrons, and to apply them to physical properties of Al-transition-metal alloys.

It is difficult to develop simple, accurate descriptions of bonding energetics in Al-transition-metal alloys, because Al is free-electron-like, but the  $d$  orbitals which dominate transition-metal bonding are fairly localized. Thus, neither free-electron perturbation theory nor tight-binding analysis can by itself treat these systems. Hybrid perturbative approaches have been developed<sup>3</sup> for incorporating  $d$  shells in nearly-free-electron systems, but these have not, to our knowledge, been applied to alloys. However, structural stability in Al-rich Al-transition-metal alloys has been studied with the effective-medium theory (EMT).<sup>4-6</sup> This approach begins with the energy associated with embedding a single transition-metal atom in a uniform electron gas. Radial corrections are then obtained which take into account the discrete nature of the Al lattice. This method has produced structural energy differences which are consistent with some of the observed structures. The results were explained essentially

on the basis of environmentally dependent atomic-size effects. Unfortunately, the EMT provides no way for us to probe the electronic origins of the various energy differences, and does not in its present form include angular forces, which are very important in transition-metal-rich alloys.

Several quantitative band-theoretic total-energy calculations have also been performed for ordered Al-transition-metal compounds and closely related systems. A study of the ordered compounds in the Al-Ni system has been made<sup>7</sup> with the augmented-spherical-wave (ASW) method, supplementing an earlier calculation<sup>8</sup> for NiAl. It was found that the  $d$ -band energy accounts for most of the heat of formation of the Ni<sub>3</sub>Al and NiAl compounds, but that the conduction electrons contribute significantly in Al<sub>3</sub>Ni. A subsequent systematic study<sup>9</sup> of the bonding interactions between first-row  $s$ - $p$  elements and transition metals led to a model emphasizing two effects. The first is the "expansion energy" associated with inserting the  $s$ - $p$  atom into the metal lattice, which is always positive and has a maximum as a function of the number of  $d$  electrons at close to a half-filled  $d$  band. The second is the covalent-bonding energy, which has its largest (negative) magnitude when the  $sp$ - $d$  complex is close to half-filled and the energy separation between the  $s$ - $p$  valence levels and the  $d$  levels is relatively small. Because Al is considerably larger than the first-row atoms, this model cannot be directly applied to the Al-transition-metal systems, although we shall see that a modified version of it explains our results quite well. A few calculations<sup>10,11</sup> have treated more subtle problems, such as the relative stabilities of the  $L1_2$  and  $D0_{22}$  structures in Ni<sub>3</sub>Al and Al<sub>3</sub>Ti. In addition, cluster interactions have been obtained<sup>12-14</sup> for the Al-Ni system via input from quantum-mechanical supercell total-energy calculations, and mean-field methods based on multiple-scattering theory have been used<sup>11</sup> to calculate pair and triplet Ising-type interactions in the Al-Ni and Al-Ti systems. In all cases, strong ordering tendencies were ob-

served, with the Al-Ni interactions very short ranged and the Al-Ti interactions somewhat longer ranged.

However, no global picture of the bonding properties of Al-transition-metal alloys has yet emerged. We attempt to supply such a picture by performing a systematic series of calculations of nearest-neighbor Ising-type cluster interactions for ordering properties of these alloys on a parent fcc lattice. We treat alloys of Al with all of the 3*d* and 4*d* transition metals; we do not treat the 5*d* row because of the complications of relativistic effects. The interactions, which are calculated through the tetrahedron level, are obtained by matching to the results of supercell-compound total-energy calculations on a parent fcc lattice, as in Ref. 12. Our results extend the previous calculations on ordered compounds both in their scope and in our emphasis on interaction parameters, which can describe a variety of physical properties. They differ from the muffin-tin-based multiple-scattering theory results in the method of obtaining the interactions; our reasons for using the matching method are discussed in Sec. II. The use of the fcc underlying lattice is, of course, somewhat restrictive, since many of the alloys have only a restricted range of fcc solubility. However, the use of a single underlying lattice shows in the clearest fashion the dependence of the values of the interaction parameters on the transition-metal *d*-electron count. Furthermore, we find that the dominant factors determining the interaction parameters are simple enough to be independent of the lattice. In fact, results<sup>13</sup> for the Ni-Al system have revealed little difference between fcc and bcc interaction parameters, except for the expected variation with bond length. Thus, a considerable amount of insight can be gained from the fcc calculations. Furthermore, there is always a small but finite region of fcc solid solution at the Al end of the phase diagram, and our results are essential for in determining the extent of this region.

We find that the dependence of the pair interactions on the transition-metal *d* count can be understood in a simple fashion in terms of the width and shape of the density of states induced by the transition-metal *d* orbitals. The contribution from the *d*-band *width* leads to values of the pair interaction that favor ordering in all cases. The contribution from the *d*-band *shape* enhances the ordering tendency for early and late transition metals, but inhibits it for transition metals close to the center of the row. This picture is quite similar to that developed in Ref. 9 for boron-transition-metal compounds except that the "expansion energy" of Ref. 9 is replaced by one contribution to our bandwidth term. We associate the bandwidth and band-shape contributions to the pair interactions with the second and fourth moments, respectively, of a model density of states, and find that the resulting densities of states are quite similar to those that emerge from our calculations.

In addition to providing insight into the basic physics of the bonding processes, the cluster interactions can be used to calculate several directly observable properties. We present results for heats of solution, solid solubilities, and short-range order. For most of the systems treated, these are the first such results that have been presented.

Heats of solution for the Ni-Al system have previously been obtained<sup>12</sup> using essentially the method we use here. A strong asymmetry was found between the Al and Ni ends of the phase diagram, consistent with the present results for several other systems. In addition, heats of solution, phase diagrams, and short-range-order parameters have been obtained<sup>11,15</sup> via the mean-field multiple-scattering techniques mentioned above, for a few systems having small atomic-size mismatches. The results presented here constitute the first systematic study for Al-transition-metal alloys. The heat of solution for small concentrations is obtained as a linear combination of the cluster interactions, with corrections for long-ranged interactions, and atomic-size and lattice-relaxation effects. For all of the systems for which data are available, except for Al-Ag, we find rapid convergence of the cluster expansion and good agreement with experiment; for Al-Ag the *d*-band effects and thus the heat of solution are small, and the nearest-neighbor approximation is a poor starting point. We evaluate a simple expression for the solid solubility (in low-solubility systems) in terms of the calculated heat of solution and the heat of formation of the competing ordered compound. Our results confirm the very small solubilities universally observed at the Al end of the phase diagram, as well as the higher solubilities at the transition-metal end. The effective pair interactions we obtain for short-range-order properties are strongly concentration dependent and, in several cases, change sign with varying concentration. Instead of calculating short-range-order properties directly, we compare our results to values of effective pair interactions obtained from measured short-range-order parameters via the "inverse Monte Carlo" method<sup>16</sup> and from analysis of phase diagrams. The magnitude and concentration dependence of our calculated interaction parameters are consistent with the "measured" interactions, and with the structures of some metastable fcc solid-solution phases.

The organization of the paper is as follows. In Sec. II, we briefly outline the methods used to obtain the cluster interactions and the input supercell total energies. In Sec. III we present the calculated cluster interactions and analyze their independence on the transition-metal *d* electron count. In Sec. IV, we present results for heats of solution, solubilities, and short-range order, and a comparison with available experimental results. In Sec. V we summarize our conclusions and investigate possibilities for improvement on our model.

## II. METHOD

To obtain the cluster interactions, we employ the matching method described in Ref. 17. Only the case of an underlying fcc lattice is treated. One assumes that the zero-temperature bonding energy (per atom) of an ordered or disordered collection of *A* and *B* atoms can be approximated by an expression of the form

$$E_b = V_+ V_1 \langle \sigma_i \rangle + V_2 \langle \sigma_i \sigma_j \rangle + V_3 \langle \sigma_i \sigma_j \sigma_k \rangle + V_4 \langle \sigma_i \sigma_j \sigma_k \sigma_l \rangle . \quad (1)$$

Here,  $\sigma_i$  is a spinlike variable which is 1 (−1) for an  $A$  ( $B$ ) atom, and the averages are taken over all sites, nearest-neighbor pairs, nearest-neighbor triangles, and nearest-neighbor tetrahedra. We have no *a priori* reason for the neglect of other coupling terms; the primary justification is the rapid convergence obtained already at this level, which will be demonstrated in Sec. III. The  $V_i$  are the cluster-interaction parameters. These are defined explicitly in Ref. 18 in terms of an inner product involving the alloy configurational energy and orthogonal polynomials containing the spin variables on various alloy sites. Since the exact evaluation of such expressions is computationally prohibitive, we instead choose a simpler approach in which the  $V_n$  are obtained approximately from a relatively small number of quantum-mechanical total-energy calculations.

One first calculates the band-theoretic total energies per atom,  $E_m$  ( $1 \leq m \leq 5$ ), of five ordered structures having the fcc parent structure: pure  $A$  and pure  $B$ ,  $A_3B$  and  $AB_3$  in the  $\text{Cu}_3\text{Au}$  structure, and  $AB$  in the  $\text{CuAu}$  structure (with ideal  $c/a$  ratio). By forcing the total energies obtained from the  $V_n$  to agree with the band-theoretic total energies, one obtains the  $V_n$  uniquely as functions of the  $E_m$ ;

$$V_n(a) = \sum_{m=1}^5 \xi_{n,m}^{-1} E_m(a).$$

where  $\xi_{n,m}$  is a coefficient matrix given in Ref. 17.

We employ two treatments of lattice-relaxation effects.

(1) "Frozen lattice." The properties of an alloy at a concentration determined by  $\langle \sigma \rangle$  are calculated for a perfect fcc lattice having the lattice constant corresponding to this concentration. The input total energies  $E_m$  are evaluated at this lattice constant. No *local* relaxation effects are included.

(2) "Locally relaxed." It is now assumed that small clusters of atoms in the alloy can have their preferred lattice constant. Thus the input total energies  $E_m$  are evaluated at their zero-pressure lattice constants, rather than the average alloy lattice constant. This procedure tends to reduce the ordering tendency (cf. Sec. IV C), since the energy penalty paid for separating the alloy into its constituents is reduced by allowing these constituents to have their preferred lattice constants.

The "locally relaxed" treatment is probably more accurate than the "frozen-lattice" treatment; the latter gives too high an energy for a random alloy, since the neglected local lattice relaxations provide a stabilizing contribution to this energy. Thus our results for the heats of solution, solid solubilities, and short-range order include the local relaxation effects. However, in analyzing the electronic contributions we will find it convenient to temporarily ignore these effects, using the "frozen-lattice" treatment. In addition, in calculating the heats of solution we isolate the relaxation effects by first performing frozen-lattice calculations and subsequently evaluating the relaxation energy as the difference between the locally relaxed estimate and the frozen-lattice estimate.

The supercell total energies are calculated using the augmented-spherical-wave (ASW) method.<sup>8</sup> We employ

an exchange-correlation functional of the Hedin-Lundqvist form.<sup>19</sup> We neglect magnetic and relativistic effects. For Al we use a basis set of 3s, 3p, and 3d ASW's, for the 3d transition metals the 4s, 4p, and 3d ASW's, and for the 4d transition metals the 5s, 5p, and 4d ASW's. Equal ASW sphere radii are used for each of the constituents in the compound calculations. This choice of sphere radii is based on the optimal partitioning of space into overlapping spheres. The smallness of the overlap volume of the spheres is a measure of the quality of the partitioning. The choice of equal sphere radii gives an overlap volume of only 7.9% of the total volume, which is a local minimum as a function of the sphere radii. One could envisage choosing the sphere radii to minimize the calculated total energy. Provided that the energy functional were correct, this would provide an optimal charge density and energy. However, the energy functional itself is approximate, since it is based on a sphericalized charge density. The error in the functional then also depends on the sphere radii. Therefore there is no guarantee that the sphere radii which minimize the calculated total energy result is an optimal charge density or total energy. We consider the geometric criterion of minimizing the overlap volume to be more reliable.

Our main reason for using the matching approach rather than the mean-field multiple-scattering methods<sup>11,15</sup> is that many of the Al-transition-metal alloys have large atomic-size mismatches, which renders the mean-field methods difficult to apply. While the multiple-scattering methods can, in principle, treat arbitrary atomic-size ratios, their implementations have used muffin-tin potentials with equal sphere radii. In systems with large atomic-size mismatches, this leads to substantial charges inside the spheres. The effects of the interaction of these charges are naturally included in band-structure calculations for periodic systems, but have not yet been included in their entirety in calculations for random systems. Additional justification for the use of the matching method comes from the expectation that the interactions in Al-transition-metal alloys should be short ranged, because of the large electron density in Al and the damping effects due to the large difference in scattering strengths between the two constituents. This expectation is confirmed by our estimates of long-ranged contributions to the heats of solution (cf. Sec. IV A).

### III. CHEMICAL TRENDS IN VALUES OF INTERACTION PARAMETERS

Our intent in this section is to analyze in a simple fashion the dependence of the interaction parameters on the transition-metal  $d$ -electron count and the alloy lattice constant. Figure 1 shows the calculated values of  $V_2$  for alloys of Al with 3d and 4d transition metals; positive values of  $V_2$  correspond to ordering tendencies, and, in most cases, to exothermic heats of formation. Results for both the frozen-lattice and locally relaxed treatments are shown. Although several of the 3d transition metals have large magnetization energies, we include the paramagnetic results here in order to make the dependence on the transition-metal  $d$  count as transparent as possible. We

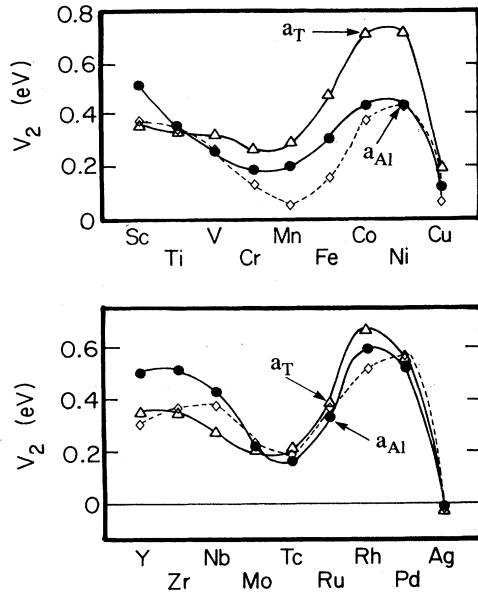


FIG. 1. Pair interactions for alloys of Al with (a) 3d and (b) 4d transition metals. Curves labeled  $a_T$  and  $a_{Al}$  are obtained using the frozen-lattice treatment, at transition-metal and Al lattice constants, respectively. Dashed curves are obtained by use of the locally relaxed treatment.

note that for all the transition metals with partly filled  $d$  shells,  $V_2$  is large and positive. The sign of  $V_2$  implies that, if forced to reside on a hypothetical fcc lattice, all of these alloys would display compound formation in same temperature and concentration range, since compound formation reduces  $\langle \sigma_i \sigma_j \rangle$  [cf. Eq. (1)]. The magnitude, in turn, implies that many of these compounds would remain ordered up to the melting temperature. For example, neglecting the higher-order interactions, the order-disorder temperature for the CuAu phase<sup>20</sup> is approximately  $0.3V_2/k_B$ , which ranges from 600 to 2400 K for the systems considered here; by comparison, the melting temperature of Al is 933 K and those of the partly-filled-shell 3d and 4d transition metals range<sup>21</sup> from 1795 to 2890 K. Since many Al-transition-metal-compounds form on parent lattices other than the fcc lattice, the above conclusions cannot be rigorously applied to these compounds; nevertheless, the conclusions are suggestive and are consistent with the observed phase diagrams,<sup>21</sup> all of which display ordered compounds up to the melting temperature (except for the Al-Tc and Al-Rh systems, for which, to our knowledge, no reliable phase diagram has been measured).

The large positive values of  $V_2$  suggest that changes in the one-electron density of states are the dominant exothermic contribution to  $V_2$ . The other likely major exothermic contribution would result from ionic charge-transfer effects. We have shown that the charge-transfer (CT) contribution  $\Delta H^{CT}$  is smaller than the one-electron band contribution, using a crude quadratic model which neglects changes in the density of states due to interactions between the alloy constituents. We consider the

CuAu structure for simplicity, and evaluate  $\Delta H^{CT}$  per Al-transition-metal pair. If the amount of electron transfer from the Al sites to the transition-metal ( $T$ ) sites is denoted by  $\Delta q$  the part of  $\Delta H^{CT}$  that is linear in  $\Delta q$  is

$$\Delta H^{(1)} = \Delta q (\epsilon_F^T - \epsilon_F^{Al}) .$$

Here,  $\epsilon_F^T$  and  $\epsilon_F^{Al}$  are the Fermi levels for the transition metal and Al, in the absence of surface dipole effects. There are two terms in  $\Delta H^{CT}$  that are quadratic in  $\Delta q$ . The first results from the constraint of single occupancy of the one-electron states. If  $\Delta q > 0$ , then the electrons that move to the transition-metal sites must be placed at progressively higher energies, and are taken from lower energies on the Al sites. The contribution from this effect is readily seen to be

$$\Delta H^{(2),a} = \frac{1}{2} \Delta q^2 (\rho_T^{-1} + \rho_{Al}^{-1}) ,$$

where  $\rho_T$  and  $\rho_{Al}$  are the transition-metal and Al Fermi-level densities of states per atom. The second quadratic term results from the increase in electrostatic energy due to charge transfer. It is given by

$$\Delta H^{(2),b} = \Delta q^2 (U_T + U_{Al}) - \alpha (\Delta q)^2 e^2 / R ,$$

where  $U_T$  and  $U_{Al}$  are the interatomic Coulomb integrals for states at the Fermi level,  $\alpha$  is the Madelung constant, and  $R$  is the Al-transition-metal spacing. Minimizing the total  $\Delta H^{CT}$  with respect to  $\Delta q$ , one obtains

$$\Delta q^{(min)} = (\epsilon_F^{Al} - \epsilon_F^T) (\rho_T^{-1} + \rho_{Al}^{-1} + 2U_T + 2U_{Al} - 2\alpha e^2 / R)^{-1}$$

and

$$\begin{aligned} \Delta H^{CT} &= \Delta H^{(1)} + \Delta H^{(2),a} + \Delta H^{(2),b} \\ &= \frac{1}{2} \Delta q^{min} (\epsilon_F^T - \epsilon_F^{Al}) . \end{aligned}$$

A rough upper bound on  $|\Delta H^{CT}|$  is obtained as follows. Typical transition-metal bandwidths are 5 eV or greater, so that we choose  $\rho_T = 2 \text{ eV}^{-1}$ ; larger bandwidths will result in a smaller value of  $|\Delta H^{CT}|$ . For  $\rho_{Al}$ , we take the free-electron value of  $0.4 \text{ eV}^{-1}$ . The Coulomb integrals are approximately obtained from charge densities  $\bar{\rho} = \Omega^{-1}$  uniformly distributed over the atomic spheres, so that

$$\begin{aligned} U_T = U_{Al} &= \frac{e^2}{2} \frac{1}{\Omega^2} \int d^3r d^3r' |r - r'|^{-1} , \\ &= \frac{3}{5} e^2 / R_{WS} , \end{aligned}$$

where  $\Omega$  is the volume of the atomic sphere,  $R_{WS}$  is the radius of the atomic sphere (or the Wigner-Seitz radius), and the integrals are carried out only over the atomic sphere. The use of realistically localized  $d$  charge densities for the transition-metal sites would likely increase  $U_T$  and thus reduce  $|\Delta H^{CT}|$ . The Madelung constant for the CuAu structure, which we obtain as a special case of the ASW structure constants,<sup>8</sup> is 1.59. At the Al lattice constant of 4.05 Å, we have  $R = 2.86 \text{ Å}$  and  $R_{WS} = 1.58 \text{ Å}$ , so that

$$(\rho_T^{-1} + \rho_{Al}^{-1} + 2U_T + 2U_{Al} - 2ae^2/R) = (0.5 \text{ eV} + 2.5 \text{ eV} + 10.9 \text{ eV} + 10.9 \text{ eV} - 16.0 \text{ eV}) = 8.8 \text{ eV} .$$

The Fermi levels  $\epsilon_F^T$  and  $\epsilon_F^{Al}$  cannot be measured directly, since measured work functions include surface dipole effects. However, the Fermi levels are closely related to the electronegativity  $X$ , and a relation  $\epsilon_F = -2.27X + (\text{const})$  has been obtained,<sup>22</sup> for  $\epsilon_F$  given in eV. The electronegativity differences<sup>23</sup> between Al and the transition metals considered here do not exceed 0.7, so that we expect  $|\epsilon_F^T - \epsilon_F^{Al}| \leq 1.6$  eV. We then have  $|\Delta q| \leq 0.18$  and  $|\Delta H^{CT}| \leq 0.14$  eV. This results in a contribution of magnitude 0.05 eV to  $V_2$ , which is much smaller than the values shown in Fig. 1. Thus it is likely that electronic band effects are the major exothermic contribution to  $V_2$ .

The values of  $V_2$  for Ag and, to a lesser extent, Cu, are significantly smaller than for the partly-filled-shell systems. This difference is reflected in the experimental heats of formation,<sup>24</sup> to be described in Sec. IV. We believe that the smaller magnitude of  $V_2$  is due to the almost complete filling of the  $d$  shell, which renders it to some extent inert (although  $s$ - $d$ -hybridization effects contribute significantly to the cohesive energies of both of these metals). Since the  $d$  bands in Ag lie farther below the Fermi energy  $\epsilon_F$  than those in Cu, this contention is supported by the smaller value of  $V_2$  in Ag relative to that in Cu.

In the systems with the largest atomic-size mismatches, the lattice-constant effects on  $V_2$  can also be quite large.  $V_2$  increases with decreasing lattice constant. In Al-Co and Al-Ni, the frozen-lattice values at the Al lattice constant are nearly 50% smaller than at the shorter transition-metal lattice constant. The early  $4d$  transition metals have larger lattice constants than Al (when forced to reside on a fcc lattice); in these cases  $V_2$  is larger at the Al end. Phase-diagram calculations<sup>12</sup> for Al-Ni, using frozen-lattice interactions, show that large asymmetries in the phase diagram can result from the lattice-constant dependence of the interactions. The locally relaxed values in Fig. 1 are typically lower than the frozen lattice values for the shorter lattice constant; in some of the Al  $3d$  transition-metal alloys they are significantly lower than the frozen-lattice values at both the Al and transition-metal lattice constants.

A great deal about the nature of the bonding in this class of alloys can be learned by examination of the dependence of  $V_2$  on the number of  $d$  electrons,  $N_d$ , of the transition-metal component. To focus attention on the systematic trends in the electronic band energy, we consider only the values at the Al lattice constant. The calculated values of  $V_2$  for both the  $3d$  and  $4d$  rows display a minimum at a roughly half-filled  $d$  band, and, as mentioned above, drop off when the  $d$  band becomes nearly filled or nearly empty. Two maxima are seen, between the half-filled-band case and the filled- and empty-band cases. An interpretation of these effects emphasizing the width and shape of the  $d$ -band density of states (DOS) is suggested both by the large energy scale of  $V_2$

and its strong sensitivity to the  $d$ -band count, particularly its reduced magnitude for nearly filled or nearly empty bands. The width and shape of the density of states are conveniently discussed using model densities of states which are nonzero only over a finite energy interval. The gross properties of a model density of states  $\rho_d$  are described by its low-order moments:

$$\mu_n = \int_{-\infty}^{\infty} E^n \rho_d(E) dE .$$

(These cannot be calculated directly from the full band-theoretic densities of states. The latter decay too slowly at large energies for the moment integrals to be finite.) The second moment  $\mu_2$  is associated with the bandwidth. An increase in  $\mu_2$  is expected to lower the bonding energy  $E_b$  (increase the stability) of the  $d$ -band electrons because the energies of the occupied bonding states are lowered. The form of the dependence of this energy change  $\partial E_b / \partial \mu_2$  on the  $d$ -band filling has been evaluated in several model calculations,<sup>25-27</sup> which obtain a nearly parabolic shape. In Fig. 2(a) we show typical results obtained using a model DOS of the "maximum-entropy" form.<sup>27,28</sup> The maximum occurs for a half-filled band and  $\partial E_b / \partial \mu_2$  vanishes for empty or filled bands.

Once  $\mu_2$  is specified, the higher-order moments describe the *shape* of the band. Of particular interest to us is  $\mu_4$ ; the small asymmetry in  $V_2$  versus band filling suggests that  $\mu_3$  is less important. For a given value of  $\mu_2$ , a small value of  $\mu_4$  typically corresponds to a density of states having two well-defined bonding and antibonding peaks, separated by a dip or quasigap (cf. Fig. 3). Very little of the weight in the band resides outside the bonding and antibonding peaks. On the other hand, a density of states with a large  $\mu_4$  is dominated by a central peak with large contributions to  $\mu_4$  from the tails. Thus a band which is nearly empty will prefer a large  $\mu_4$ , since all of the electrons can be accommodated in the tails of the density of states; a nearly filled band will also prefer a large  $\mu_4$  for similar reasons. On the other hand, a half-filled band will prefer a small  $\mu_4$  since then the Fermi level  $\epsilon_F$  can reside in the quasigap, which, in general, has a stabilizing effect. As with  $\mu_2$ , a number of model calculations have suggested a shape for  $\partial E_b / \partial \mu_4$ , similar to that shown in Fig. 2(b), which is again obtained from the "maximum-entropy" model.<sup>27,28</sup> While the exact shape of  $\partial E_b / \partial \mu_4$  depends on the type of model density of states used, the presence of two zeros in this function is rigorously necessary for any density of states.<sup>25,29</sup>

Using these observations, it is possible to "Fourier analyze" the  $N_d$  dependence of  $V_2$  (cf. Fig. 1) by separating it into contributions from the various moments of  $\rho_d$ . The uniformly positive values of  $V_2$  (recall that positive  $V_2$  corresponds to a negative heat of mixing) would suggest an increase in  $\mu_2$  upon mixing, while the peaks above and below the half-filled band correspond to an increase in  $\mu_4$ . As shown in Fig. 2(c), the  $N_d$  dependence observed in

Fig. 1 can, in fact, be reasonably well reproduced by a sum of contributions from  $\mu_2$  and  $\mu_4$ . (There is a sign difference between these figures because positive values of  $V_2$  correspond to negative heats of formation.) These observations would suggest that  $\rho_d$  is broadened in the Al environment relative to the pure transition metals, and that more of its weight should be contained in its tails. This contention is supported by comparison of the model DOS with the calculated ones for the Al-Ni system shown in Fig. 3. In Fig. 3(b) we have subtracted off the free-electron background DOS in order to focus on the DOS  $\rho_d$  induced by the  $d$  orbitals. We see that the  $\rho_d$  plots for  $\text{Al}_3\text{Ni}$  and Ni compare favorably with the solid and dashed curves in Fig. 3(a), respectively. The DOS shown by the solid curve has a value of  $\mu_2$  larger by 40% than that of the dashed curve, and a value of  $\mu_4$  50% larger [when scaled by  $(\mu_2)^2$ ]. These values are sufficient to roughly account for the values of  $V_2$  seen in Fig. 1.

Our observations regarding the width of the DOS are consistent with the fact that Al reduces magnetic moments on transition-metal ions, which suggests a larger

$d$ -band width in the Al matrix. Both free-electron and tight-binding analysis would also suggest larger values of  $\mu_4$  in the Al environment, corresponding to significant tailing of the band. If a  $d$ -electron impurity is embedded in a free-electron gas, one obtains (at least in the weak-coupling limit) a Lorentzian shape for  $\rho_d$ . This has a much larger fraction of its weight in the tails than in pure transition metals, in which the  $d$ -band density of states is closer to rectangular in shape. On the other hand, in tight-binding analyses pure transition metals have fairly small values of  $\mu_4$  [when scaled by  $(\mu_2)^2$ ] because of phase cancellation effects resulting from the rapid angular dependence of the  $d$  orbitals. For example,<sup>27</sup> typical values of the dimensionless fourth moment  $\gamma_4 = \mu_4 \mu_0 / (\mu_2)^2$  for  $d$ -band models of transition metals are roughly 2, while corresponding  $s$ -band models (which do not exhibit phase-cancellation effects) have  $3 \leq \gamma_4 \leq 4$ . We would expect  $p$  orbitals to display a behavior intermediate between  $s$  and  $d$  orbitals. Thus, since the electronic structure of Al is dominated by  $s$  and  $p$  orbitals,  $\gamma_4$  for a  $d$  orbital embedded in Al should be larger than in a pure transition metal.

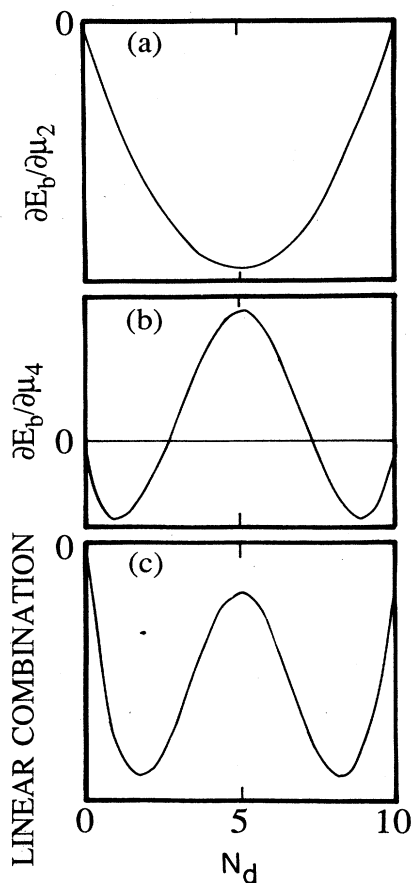


FIG. 2. Dependence of bonding energy on (a) second and (b) fourth moments of electronic density of states, in a maximum-entropy reconstruction (Ref. 27). Panel (c) shows a linear combination with coefficients chosen to simulate behavior of  $V_2$  in Fig. 1.

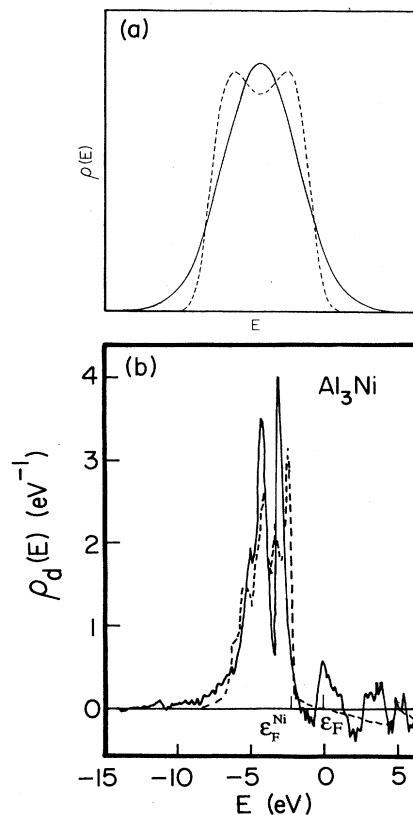


FIG. 3. (a) Model densities of states generated by maximum-entropy method (Ref. 27). Solid curve has larger values of  $\mu_2$  (by 40%) and  $\mu_4 \mu_0 / (\mu_2)^2$  (by 50%) than dashed curve. (b) Density of states induced by  $d$  orbitals, per Ni atom, in (fcc)  $\text{Al}_3\text{Ni}$ . Dashed curves indicates induced  $d$  density of states in pure Ni;  $\epsilon_F^{\text{Ni}}$  is Fermi level for pure Ni.

The present description of the bonding energetics, in its focus on the  $d$  band and its interaction with the Al  $s$ - $p$  complex, is similar to that of Ref. 9. However, because we consider substitutional alloys, in which the transition-metal–transition-metal bond *number*, rather than bond *length*, changes, we cannot directly transfer the “expansion-energy” contribution from that analysis. Nevertheless, the present model may be thought of in terms of two steps, in which transition-metal–transition-metal bonds are first broken and subsequently replaced by transition-metal–Al bonds. The bond-breaking part of this process is a repulsive term closely analogous to the “expansion energy” of Ref. 9 in the sense that the latter comes from weakened, rather than broken, bonds. In fact, their  $N_d$  dependences are both roughly parabolic.

Figure 4 shows the calculated values of  $V_3$  versus  $d$ -band filling. The overall energy scale of  $V_3$  is roughly 5 times smaller than that of  $V_2$ , indicating fairly rapid convergence of the cluster expansion. However, the values of  $V_3$  seen here are sufficient to significantly perturb the phase diagram.<sup>12</sup>  $V_3$  oscillates quite rapidly with the  $d$ -band filling, having three zeros inside the  $d$  band. By employing arguments similar to those applied above to  $V_2$ , one can show that this behavior is consistent with a large contribution from  $\mu_5$ . The sign of this contribution is such that systems having large values of  $\langle \sigma_i \sigma_j \sigma_k \rangle$  have low values of  $\mu_5$ . The dependence of  $V_3$  on the lattice constant is even stronger than that of  $V_2$ ; for several of

the transition metals the frozen-lattice values of  $V_3$  change by more than a factor of 2 between the Al and transition-metal lattice constants. The locally relaxed values have roughly the same band-filling dependence as the frozen-lattice values.

For comparison, we include in Fig. 4 estimates of  $V_3$  obtained from the asymmetry of the calculated heats of solution in the “Miedema” model.<sup>30</sup> The Miedema values are too small and do not display the oscillations that we find. We believe that this is because the heat-of-formation asymmetry in the Miedema model includes only atomic-size effects. The present results indicate that the electronic band contribution can significantly exceed the atomic-size effects.

The values of the tetrahedron interaction  $V_4$  are, in general, several times smaller than those of  $V_3$ . The behavior of  $V_4$  exhibits quite rapid variations as a function of  $N_d$ , but these are much less regular than those of  $V_2$  and  $V_3$ . We do not have a simple interpretation of this behavior in terms of the moments of  $\rho_d$ , such as that for  $V_2$  and  $V_3$ .

#### IV. APPLICATIONS OF CLUSTER INTERACTIONS

In this section we use the values of the cluster interaction calculated in the preceding section to calculate several types of thermodynamic properties of Al–transition-metal alloys. To our knowledge, these are the first nonempirical calculations of these properties except for the heat of solution,<sup>12</sup> and the pair interactions<sup>11</sup> for describing short-range order, in the Ni–Al system.

##### A. Heats of solution

We treat the limit of small concentration. Although our final results include the local relaxation effects, we find it convenient to isolate these effects by starting with a term evaluated in the frozen-lattice approximation. The following model for the heat of solution per solute atom  $\Delta H$  is used:

$$\Delta H^{SS} = \Delta H^{NN} + \Delta H^{LR} + \Delta H^{el} + \Delta H^{rel}. \quad (2)$$

The first two terms on the right-hand side of (2) are evaluated at the host lattice constant and denote contributions from the nearest-neighbor interactions  $V_0$ – $V_4$  and longer-ranged terms, respectively. The third term denotes the elastic strain energy associated with compressing the solute atom to the host lattice constant. The last term contains an estimate of the contribution due to local lattice relaxations. Since the correlation functions in (1) are  $\pm 1$  in the pure-metal phases and powers of  $\langle \sigma \rangle$  in the random solid solution, we have

$$\Delta H^{NN} = -4(V_2 + \langle \sigma \rangle V_3 + 2V_4), \quad (3)$$

where  $\langle \sigma \rangle = 1$  ( $-1$ ) for a transition-metal (Al) host, and the  $V_n$  are evaluated at the host lattice constant with no local relaxation effects included. The primary purpose of the  $\Delta H^{LR}$  term is to evaluate the error resulting from the nearest-neighbor approximation. We approximate it by calculating in two ways the heat of formation for an ordered supercell structure having solute atoms at one-

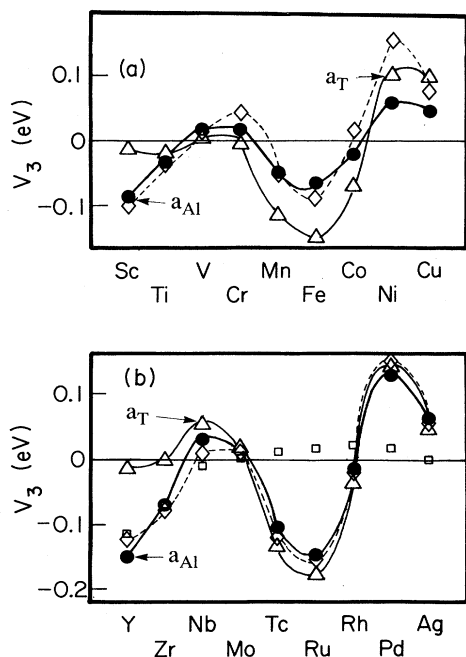


FIG. 4. Triplet interactions for alloys of Al with (a) 3d and (b) 4d transition metals. Curves labeled  $a_T$  and  $a_{Al}$  are obtained using the frozen-lattice treatment, at transition-metal and Al lattice constants, respectively. Dashed curves are obtained by use of the locally relaxed treatment. Squares in (b) denote values from “Miedema” method (Ref. 30).

eight of its sites, obtained by doubling the primitive fcc unit cell in all directions. (This structure is not included in the input database for the  $V_n$ ). We first obtain the heat of formation per solute atom via a full quantum-mechanical calculation using the same techniques that were used to generate the  $E_m$  (cf. Sec. II). This quantity is denoted  $\Delta H_8^{\text{QM}}$ . We define  $\Delta H^{\text{LR}}$  as the difference  $\Delta H_8^{\text{QM}} - \Delta H_8^{\text{NN}}$ , where  $\Delta H_8^{\text{NN}}$  is the estimate of the heat of formation obtained by the nearest-neighbor parameters. The elastic energy  $\Delta H^{\text{el}}$  is approximated as the energy difference per atom between a fcc lattice of solute atoms at the host lattice parameter and the same lattice at the solute lattice parameter; these energies are again obtained by the quantum-mechanical techniques described in Sec. II. To obtain the relaxation energy  $\Delta H^{\text{rel}}$ , we first estimate the nearest-neighbor contribution to the heat of formation using the *locally* relaxed  $V_n$ .  $\Delta H^{\text{rel}}$  is then defined as the difference between this estimate and that given by  $\Delta H^{\text{NN}} + \Delta H^{\text{el}}$ .

Figure 5 shows results for the subset of the alloys for which reliable heats of solution are available. Although many transition metals dissolve considerable amounts of Al, most have very low solubilities in Al; only for Ag is heat-of-solution data available for the Al-rich phases. The  $\Delta H^{\text{rel}}$  contribution is not shown explicitly because it is too small to be seen on the scale of the figure ( $|\Delta H^{\text{rel}}| \leq 0.05$  eV in all cases shown). Ni and Pd display the most exothermic values of  $\Delta H^{\text{NN}}$  at the transition-metal-rich end, with the values for Ti and Cu being roughly half as large. The values for Ag-Al solutions at both ends of the phase diagram are considerably smaller in magnitude, as expected from the small values of the interaction parameters. The endothermic value of  $\Delta H^{\text{NN}}$  at the Al-rich end, in particular, indicates that this sys-

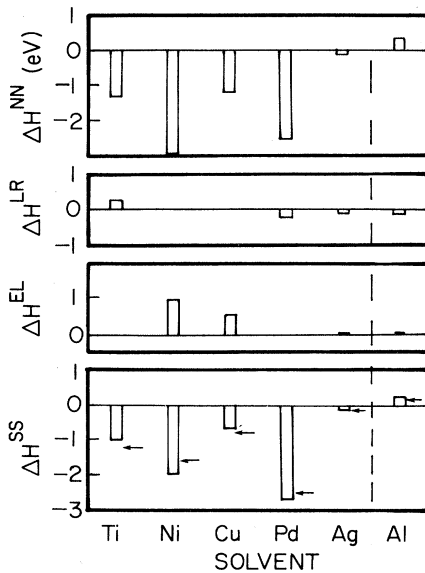


FIG. 5. Contribution to heat of solution  $\Delta H^{\text{SS}}$  [cf. Eq. (2)], for Al dissolved in Ti, Ni, Cu, Pd, Ag, and Ag dissolved in Al. Arrows denote experimental values (Ref. 24).

tem is dominated by physical mechanisms considerably different from those in the partly-filled- $d$ -shell systems. With the exception of the Ag-Al system, we have  $|\Delta H^{\text{LR}}| \ll |\Delta H^{\text{NN}}|$ , which speaks favorably for the convergence of the cluster expansion. In fact, the nearest-neighbor results, without  $\Delta H^{\text{LR}}$ , agree as well with the experimental results as those with  $\Delta H^{\text{LR}}$ . The elastic energy  $\Delta H^{\text{el}}$  is also considerably smaller than  $\Delta H^{\text{NN}}$  for most of the systems; the largest contribution is in Cu, in which it is almost half of  $\Delta H^{\text{NN}}$ .

The sum  $\Delta H^{\text{SS}}$  of these contributions matches the chemical trends in the measured values very well, and even fits the numerical values quite closely. This is somewhat surprising in the Ag-Al case, because the large magnitude of  $\Delta H^{\text{LR}}$  relative to  $\Delta H^{\text{NN}}$  would suggest that the cluster expansion converges slowly. There are a large number of possible contributions to the discrepancy with experiment, most of which we are not in a position to evaluate. The local-density approximation (LDA) for exchange and correlation is well known to give significant errors in cohesive energies, although the magnitude of the error in the energy differences of interest here is not clear. In the Ni-Al solid-solution results, the neglect of magnetic effects contributes to the overestimate of the heat of solution. Approximate inclusion of the magnetic effects, by using ferromagnetic pure Ni in the input supercell total energies, reduces the discrepancy by roughly 50%. Other possible reasons for discrepancies include lattice-vibrational energies and temperature-dependent lattice relaxations.

## B. Solid solubilities

Since the numerical values of solid solubilities are extremely sensitive to small errors in the calculated thermodynamic quantities, we express the results for this quantity in terms of an energy difference  $\Delta E$ , defined by

$$\Delta E = \Delta H^{\text{SS}} - \Delta H^{\text{ord}}. \quad (4)$$

Here  $\Delta H^{\text{SS}}$  is the heat of solution per solute atom of the low-concentration solid solution;  $\Delta H^{\text{ord}}$  is the heat of formation (per solute atom) of the ordered phase which competes with the solid solution to determine the solubility. In the limit of small solubility, one easily shows from regular-solution theory that

$$C_{\text{max}} = e^{-\Delta E/k_B T}, \quad (5)$$

where  $C_{\text{max}}$  is the solid solubility. In obtaining this result we have neglected the temperature dependence of  $\Delta E$  and the entropy of the ordered phase. The latter is very small because of the large magnitude of the ordering energies. However, since solubilities are typically evaluated at around 700 K, the temperature dependence of  $\Delta E$  is not negligible. Our results can therefore be used only to obtain chemical trends and rough magnitudes, rather than precise predictions.

To evaluate  $\Delta E$  we have used the values of  $\Delta H^{\text{SS}}$  given by Eq. (2). We can evaluate  $\Delta H^{\text{ord}}$  from our model only for cases in which the competing ordered phase has the

$\text{Cu}_3\text{Au}$  structure. Of the systems we discuss here, this includes only  $\text{Al}_3\text{Sc}$  and  $\text{Ni}_3\text{Al}$ . For other cases we have taken  $\Delta H^{\text{ord}}$  from experimental data, where available.

The results for the Al-rich and transition-metal-rich ends of the phase diagrams are shown in Figs. 6(a) and 6(b), respectively. The experimental points in panel (a) are obtained from the measured solubilities<sup>1</sup> using Eq. (5). We show data for all systems (1) for which  $\Delta H^{\text{ord}}$  has been measured or which form the  $\text{Cu}_3\text{Au}$  structure at both ends of the phase diagram, (2) in which the transition metal has the fcc or hcp structure, and (3) in which the magnetization energy is small ( $< 0.1$  eV). The most striking feature of the results for this case is the large magnitude of  $\Delta E$  when compared with typical temperatures at which solubilities are measured ( $T \approx 700$  K); for the systems shown in Fig. 6(a), we have  $4 \lesssim \Delta E/k_B T \lesssim 13$ , suggesting very small solubilities for transition metals in Al. This expectation is confirmed by the experimentally determined values of  $\Delta E$ , which have the same overall magnitude as the theoretical estimates. Although the agreement between the theoretical and experimental points is not quantitative, the chemical trends are well reproduced, with Ni having the largest value. The observed discrepancies are undoubtedly caused in part by the neglect of the temperature dependence of  $\Delta E$ , in addition to the various approximations made in calculating  $\Delta H^{\text{SS}}$ , and the experimental uncertainties in  $\Delta H^{\text{ord}}$ . For comparison we show in Fig. 6 the values that are obtained by the frozen-lattice treatment, neglecting local lattice relaxations. This raises the energy of the solid solution and thus increases  $\Delta E$ . Only in the case of

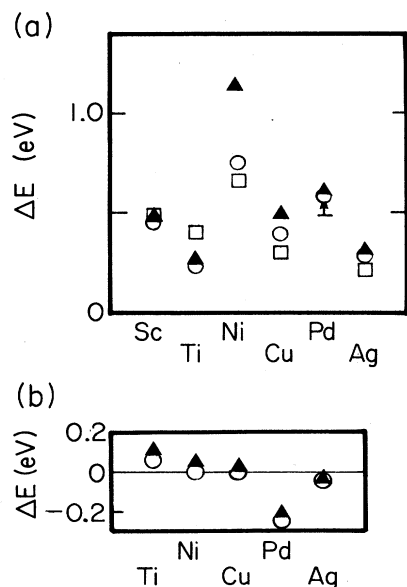


FIG. 6. Solid-solubility energy difference  $\Delta E$  [cf. Eq. (4)], for (a) Al-rich and (b) transition-metal-rich solid solutions. Circles denote calculated values; squares denote experimental values (Ref. 1); triangles denote calculated frozen-lattice values; bar and arrow for Pd in (a) denote lower limit for solubility of Pd in Al.

Ni in Al, in which  $\Delta E$  increases by 0.4 eV, does neglect of the local relaxations have a large effect.

The values of  $\Delta E$  for the transition-metal-rich case have a smaller magnitude than those for the Al-rich case, suggesting much larger solubilities at the Al-rich end. This is consistent with the experimental data, which for all the systems considered yield solubilities greater than 10% even at temperatures far below the transition-metal melting point. In fact, for all the Al-transition-metal alloys the solubility at the transition-metal end significantly exceeds that at the Al end. This certainly cannot be explained by atomic-size effects, since the atomic size of Al is neither universally larger nor smaller than those of the transition metals. One would expect the solubility to be strongly correlated with the heat of solution<sup>31</sup>  $\Delta H^{\text{SS}}$ , although the connection is not rigorous because of the competition from phases not having the fcc structure. Table I displays the asymmetries in  $\Delta H^{\text{SS}}$ ,  $\Delta H^{\text{ord}}$ , and  $\Delta E$ . For Ni, Cu, Pd, and Ag, we do find that the asymmetry in the solubility (or, equivalently,  $\Delta E$ ) is dominated by the asymmetry in  $\Delta H^{\text{SS}}$ . The latter is primarily due to the three-body interaction  $V_3$ , and to the lattice-constant dependence of the  $V_n$ . However, the correlation between the asymmetry in the solubility and that in  $\Delta H^{\text{SS}}$  breaks down for the Al-Ti and Al-Sc cases. In Al-Ti,  $\Delta H^{\text{SS}}$  is most exothermic at the Al-rich end, which would suggest a greater solubility at that end as well. However, the asymmetry in  $\Delta H^{\text{ord}}$  more than cancels that in  $\Delta H^{\text{SS}}$ . In Al-Sc we do not have measured values for  $\Delta H^{\text{ord}}$ . Nevertheless,  $\Delta H^{\text{SS}}$  is most exothermic at the Al-rich end of the phase diagram, but the solubility is greatest at the transition-metal-rich end. Therefore, the asymmetric contributions from  $\Delta H^{\text{ord}}$  must again dominate those from  $\Delta H^{\text{SS}}$ . Thus, the overall correlation between the asymmetries of the solid solubility and those of the heat of solution is not very strong.

Because of the recent interest in the complex phases of Al-Mn alloys, we have also performed a calculation for this system. This is by necessity more approximate, since the reference state for the measured heats of formation is considerably different from the hypothetical paramagnetic fcc crystal we have used to generate the interaction parameters. We add two correction terms to  $\Delta H^{\text{SS}}$  as given by Eq. (2).

(a) The magnetization energy of the solid solution, denoted  $\Delta H^{\text{mag}}$ . We have performed a spin-polarized ferromagnetic ASW calculation for  $\text{Al}_3\text{Mn}$  in the  $\text{Cu}_3\text{Au}$

TABLE I. Asymmetries in contributions to solid-solubility energy barrier  $\Delta E$ .

	$\Delta H^{\text{SS}}(\text{Al})$ $-\Delta H^{\text{SS}}(T)$	$-\Delta H^{\text{ord}}(\text{Al})$ $+\Delta H^{\text{ord}}(T)$	$\Delta E(\text{Al})$ $-\Delta E(T)$
Sc	-0.51		(> 0)
Ti	-0.21	+0.40	0.19
Ni	+1.20	-0.46	0.74
Cu	+0.68	-0.27	0.42
Pd	+1.19	-0.35	0.84
Ag	+0.42	-0.09	0.33

structure at the lattice constant which minimizes its total energy. We obtain  $\Delta H^{\text{mag}} = -0.21$  eV.

(b) The difference in energy between paramagnetic fcc Mn (the “ $\gamma$ ” phase) and the correct reference system  $\alpha$ -Mn, denoted  $\Delta H^{\text{prep}}$  (preparation). This we approximate as the sum of the latent heats<sup>32</sup> of the  $\alpha \rightarrow \beta$  and  $\beta \rightarrow \gamma$  transitions, which is 0.05 eV.

The first term on the right-hand side of Eq. (4),  $\Delta H^{\text{SS}}$ , is  $-0.39$  eV. From the measured heat of formation of  $\text{Al}_6\text{Mn}$ ,  $-1.10$  eV/Mn-atom, we obtain  $\Delta E = -0.39$  eV  $- (-1.10$  eV)  $+\Delta H^{\text{mag}} + \Delta H^{\text{prep}} = 0.55$  eV. On the other hand, at  $T = 700$  K,  $-k_B T \ln C_{\text{max}} = 0.38$  eV. Thus our theoretical estimate of  $\Delta E$  is roughly 50% too high. To our knowledge, the only other theoretical calculation relevant to  $\Delta E$  has been obtained<sup>4</sup> by the “effective-medium theory” (EMT), mentioned in Sec. I. A solid solution with a 6:1 ratio of Al to Mn was found to have an energy 0.1 eV higher per Mn atom than the  $\text{Al}_6\text{Mn}$  compound. This value is 4 times smaller than the observed  $\Delta E$ , but it is not clear that the value will be the same in the limit of small Mn concentration.

### C. Short-range order

The observed short-range (SRO) in an alloy is very directly related to the signs and magnitudes of the underlying cluster interactions. In fact, the inverse Monte Carlo (IMC) method<sup>16</sup> has recently made it practical to obtain accurate values of concentration-dependent effective pair interactions from measured SRO data. For this reason we present our results in the form of such pair interactions, rather than calculating the SRO directly. Unfortunately, the measured pair interactions are at present available only for Al-rich Al-Cu and Al-Ni alloys. However, we present results for all of the fcc transition metals, in the hope of comparing them with future experimental results.

The nearest-neighbor effective pair interactions for describing SRO are given<sup>14</sup> in terms of the concentration-independent cluster interactions as follows:

$$V_2^{\text{SRO}}(\langle \sigma \rangle) = V_2 + 3\langle \sigma \rangle V_3 + 6\langle \sigma \rangle^2 V_4. \quad (6)$$

[We remind the reader that  $\langle \sigma \rangle = 1$  ( $-1$ ) corresponds to the transition-metal (Al) end of the phase diagram.] In the high-temperature limit this type of interaction rigorously reproduces the correct SRO; the SRO parameters are, in fact, directly proportional<sup>14</sup> to  $V_2^{\text{SRO}}$ . The pair interactions  $V_2^{\text{SRO}}$  are closely related to the types of interactions obtained by the “generalized perturbation theory” (GPT),<sup>33</sup> although the latter do not use for their definition a high-temperature expansion. Our calculated interaction values are given in Table II. In calculating these we have treated lattice-relaxation effects within the locally relaxed approximation, as in the heat-of-solution and solubility calculations. The values in parentheses are the frozen-lattice values, included for comparison. The values of  $V_2^{\text{SRO}}$  are strongly concentration dependent, changing sign between the Al and transition-metal ends of the phase diagram in four of the five cases considered. The effects of lattice relaxations are fairly large for Al-Cu and Al-Ni, particularly at the Al end. The remaining

TABLE II. Effective-pair interactions  $V_2^{\text{SRO}}$  (in eV) [cf. Eq. (6)] for alloys of Al with fcc transition metals. Values in parentheses were obtained by use of the frozen-lattice approximation.

	$\langle \sigma \rangle = -1$	$\langle \sigma \rangle = 1$
Al-Ni	-0.18 (0.13)	0.66 (0.75)
Al-Cu	-0.13 (0.01)	0.39 (0.50)
Al-Rh	0.34 (0.32)	0.25 (0.25)
Al-Pd	-0.11 (-0.05)	0.78 (0.78)
Al-Ag	-0.20 (-0.21)	0.14 (0.13)

three systems have smaller atomic-size mismatches, and the local relaxation effects change  $V_2^{\text{SRO}}$  by less than 0.1 eV.

The most reliable experimental data<sup>16</sup> are for the Al-Cu system. At 85 at. % Cu the interaction is very short ranged, with the second-neighbor value 5 times smaller than the nearest-neighbor value. This provides strong support for the tetrahedron truncation employed here. The measured values at the nearest-neighbor distance are 0.29 eV (523 K) and 0.40 eV (423 K); the former value is more relevant here because  $V_2^{\text{SRO}}$  is most accurate at high temperatures and because it is more likely that equilibrium has been established in the high-temperature case. Our theoretical value at 85% Cu ( $\langle \sigma \rangle = 0.7$ ) is 0.28 eV, in excellent agreement with the 523-K experimental value. IMC data have not been obtained for Al-rich Al-Cu solid solutions because the system changes crystal structure already at small Cu concentrations. However, studies of supersaturated solutions show that at Cu concentrations of up to 2%, a solid solution forced by kinetic constraints to occupy a fcc lattice goes through initial stages of phase separation, forming so-called “Guinier-Preston” (GP) zones.<sup>34</sup> This behavior is certainly consistent with the negative *sign* of the calculated  $V_2^{\text{SRO}}$  at the Al end (cf. Table II), although we cannot ascertain the accuracy of its *magnitude*. We note that the platelike form of the GP zones is consistent with the calculated three-body interactions as well. The three-body potential for describing short-range order is given<sup>35</sup> by  $V_3^{\text{SRO}} = V_3 + 4\langle \sigma \rangle V_4$ , which is  $+0.04$  eV at the Al end of the phase diagram. Thus even though nearest-neighbor pairs of Cu atoms are preferred, a penalty is paid for forming triplets. The (100) planes which form the initial GP zones are a favorable configuration for these interactions because they contain Cu-Cu pairs but no nearest-neighbor Cu triplets.

IMC data have also been obtained<sup>36</sup> for  $\text{Ni}_{0.90}\text{Al}_{0.10}$  alloys, at several temperatures. The resulting values of  $V_2^{\text{SRO}}$  are 0.21 eV (673 K), 0.17 eV (823 K), and 0.39 eV (973 K). The large spread in these values suggests<sup>36</sup> that the short-range order in the samples does not correspond to a homogeneous state of thermal equilibrium. Our theoretical value at 90% Ni, 0.64 eV, is considerably higher than all of these. However, it is closest to the 973-K measurement, which for reasons discussed above is the most relevant one. Furthermore, we have crudely estimated the effects of the magnetization of the Ni electrons by simply adding the magnetization energy for fcc

Ni to the pure-Ni total energy used as input. The resulting value of  $V_2^{\text{SRO}}$  is 0.54 eV, in moderately good agreement with the measured 973-K value.

For Ni-Al alloys one can also obtain estimates of the pair interactions from the temperatures of ordering transitions in Al-Ni alloys. It is not possible to ascertain directly the order-disorder temperature for the  $\text{Ni}_3\text{Al}$  ( $\text{Cu}_3\text{Au}$  structure) compound, since it has not yet disordered at the melting temperature. However, an estimate of  $1723 \pm 10$  K has been obtained<sup>37</sup> by extrapolation from a series of Ni-Al-Fe alloys, which disorder below the melting temperature. If one associates this transition with a pair Ising parameter  $J$ , one has<sup>38</sup>  $J = k_B T_c / 1.8$ , and  $V_2 = 6J = 0.48$  eV. This is close to our calculated values of  $V_2^{\text{SRO}}$  at 75% Ni, which are 0.59 eV without magnetic effects and 0.49 eV with magnetic effects. In comparison, mean-field calculations<sup>11</sup> yield  $V_2^{\text{SRO}} = 0.29$  eV at 75% Ni, significantly lower than our estimates. We caution the reader that  $V_2^{\text{SRO}}$  does not rigorously describe the order-disorder transition. However, comparison<sup>36</sup> between phase diagrams calculated using up to four-body interactions and those calculated with pair interactions of the type  $V_2^{\text{SRO}}$  shows discrepancies of less than 10%. Thus the comparison  $V_2^{\text{SRO}}$  and the pair interaction obtained from an order-disorder transformation is meaningful.

To our knowledge, IMC data for pair interactions in Al-Rh, Al-Pd, and Al-Ag alloys are not yet available for comparison with our theoretical results. However, we note that Al-rich Al-Ag alloys undergo<sup>34</sup> early stages of phase expansion analogous to those of Al-Cu alloys. This is consistent with the negative sign of the calculated  $V_2^{\text{SRO}}$  at the Al end of the phase diagram.

## V. CONCLUSIONS

In this study we have applied a simple Ising-type model for the first time to a variety of physical properties of Al-transition-metal alloys. This model reproduces observed heats of solution quite well already at the nearest-neighbor level, and explains observed chemical trends in solid solubilities. We have seen that the asymmetries in the latter are sometimes, but not always, dominated by the asymmetries in the heat of solution. Furthermore, the predictions of the model are consistent with existing data on short-range order and the structure of metastable solid-solution phases in these alloys. In addition, we have seen that the dependence of the pair interactions on the transition-metal  $d$ -electron count displays a characteristic shape, having a minimum at a roughly half-filled band, which is independent of the transition-metal row. This observation suggests that the  $d$ -orbital density of states in the Al environment is broader, and more dominated by its tails, than in the transition-metal environment. These expectations have been confirmed by comparison of the calculated density of states with model densities of states having differing bandwidths and band shapes.

Future work should elaborate on this model, in three directions.

(a) Inclusion of longer-ranged interactions in the Ising model. These are necessary for example, to discriminate between various  $A_3B$  structures,<sup>39</sup> such as  $\text{Cu}_3\text{Au}$ ,  $\text{Al}_3\text{Ti}$ , and  $\text{Al}_3\text{Zr}$ , which (on a frozen underlying lattice) are degenerate in nearest-neighbor Ising models. The primary difficulty with such an extension is that the radial separation between various shells of neighbors is quite small. This means that if one obtains the interactions by matching to total energies for periodic structures, a truncation of the energy functional at the second-neighbor separation, for example could easily place significant contributions due to the actual third-neighbor interaction in the calculated second-neighbor interaction. This effect is, of course, present to some degree in our calculations as well, but is smaller because the separation in distance between the first and second shells is larger, and the second shell has only half as many atoms as the first shell.

(b) Inclusion of different underlying lattices. This is clearly necessary in order to obtain heats of solution, solubilities, and short-range-order parameters in many of these systems. Extension of the present work to bcc and face-centered-tetragonal lattices should be fairly straightforward. However, treating more complex structures having several inequivalent sites of low symmetry, such as the  $\text{Al}_3\text{Ni}_2$  structure,<sup>39</sup> will be considerably harder. These are difficult to treat with muffin-tin or atom-sphere approximations, and may well require the use of full-potential band-structure methods. While these are considerably more time consuming than the methods described here, their application to such complex structures can be expected to occur in the foreseeable future.

(c) Development of interatomic potentials. The interaction parameters obtained here describe only atomic rearrangements on a fixed underlying lattice. It would be useful to generalize these to potential-energy functions which can (approximately) describe energy differences between competing crystal structures, and defect structures as well. As was pointed out in Sec. III, the chemical trends in the interaction parameters suggest that the dominant contributions to bonding and ordering energies in these systems come from the gross properties of the electronic density of states (such as its low-order moments), rather than its detailed structure. Thus an approximate description in terms of low-order interatomic potential functions may be viable.

## ACKNOWLEDGMENTS

This work was supported by the U.S. Department of Energy under Grant No. DE-FG02-84ER45130. The author appreciates useful conversations with Werner Schweika. He is grateful to Art Williams for supplying a copy of the augmented-spherical-wave band-structure code developed at IBM and to Robert Phillips for a careful reading of this manuscript. The band-structure calculations were performed at the Production Supercomputer Facility of the Center for Theory and Simulation in Science and Engineering at Cornell University, under National Science Foundation Grant No. DMR-86-14232.

- <sup>1</sup>L. F. Mondolfo, *Aluminum Alloys: Structure and Properties* (Butterworths, Boston, 1976).
- <sup>2</sup>D. S. Shechtman, I. Blech, D. Gratias, and J. W. Cahn, *Phys. Rev. Lett.* **53**, 1951 (1984). For an overview, see C. L. Henley, *Comments Condensed Matter Phys.* **13**, 59 (1987).
- <sup>3</sup>J. A. Moriarty, *Phys. Rev. Lett.* **55**, 1502 (1985); *Phys. Rev. B* **38**, 3199 (1988).
- <sup>4</sup>A. C. Redfield and Z. Zangwill, *Phys. Rev. Lett.* **58**, 2322 (1987).
- <sup>5</sup>J. K. Nørskov and N. D. Lang, *Phys. Rev. B* **21**, 2131 (1980); M. S. Daw and M. I. Baskes, *ibid.* **29**, 6443 (1984).
- <sup>6</sup>S. M. Foiles and M. S. Daw, *J. Mater. Res.* **2**, 5 (1987).
- <sup>7</sup>D. Hackenbracht and J. Kübler, *J. Phys. F* **10**, 427 (1980).
- <sup>8</sup>A. R. Williams, J. Kübler, and C. D. Gelatt, *Phys. Rev. B* **19**, 6094 (1979).
- <sup>9</sup>C. D. Gelatt, A. R. Williams, and V. L. Moruzzi, *Phys. Rev. B* **27**, 2005 (1983).
- <sup>10</sup>J.-H. Xu, T. Oguchi, and A. J. Freeman, *Phys. Rev. B* **36**, 4186 (1987).
- <sup>11</sup>G. M. Stocks and D. M. Nicholson, in *High-Temperature Ordered Intermetallic Alloys*, Proceedings of Symposium at Materials Research Society Fall 1986 Meeting, Boston, edited by N. S. Stoloff, C. C. Koch, C. T. Liu, and O. Izumi (Materials Research Society, Pittsburgh, 1987), p. 15.
- <sup>12</sup>A. E. Carlsson and J. M. Sanchez, *Solid State Commun.* **65**, 527 (1988).
- <sup>13</sup>A. E. Carlsson, in Ref. 11, p. 39.
- <sup>14</sup>A. E. Carlsson, *Phys. Rev. B* **35**, 4858 (1987).
- <sup>15</sup>B. L. Gyorffy and G. M. Stocks, *Phys. Rev. Lett.* **50**, 374 (1983).
- <sup>16</sup>V. Gerold and J. Kern, *Acta Metall.* **35**, 393 (1987).
- <sup>17</sup>J. W. D. Connolly and A. R. Williams, *Phys. Rev. B* **27**, 5168 (1983).
- <sup>18</sup>J. M. Sanchez, F. Ducastelle, and D. Gratias, *Physica A* **128**, 334 (1984).
- <sup>19</sup>L. Hedin and B. I. Lundquist, *J. Phys. C* **4**, 2063 (1971).
- <sup>20</sup>J. M. Sanchez, D. de Fontaine, and W. Teitler, *Phys. Rev. B* **26**, 1465 (1982).
- <sup>21</sup>T. B. Massalski, J. L. Murray, L. H. Bennett, and H. Baker, *Binary Alloy Phase Diagrams* (American Society for Metals, Metals Park, OH, 1986).
- <sup>22</sup>W. Gordy and J. O. Thomas, *J. Chem. Phys.* **24**, 439 (1956).
- <sup>23</sup>L. Pauling, *The Nature of the Chemical Bond* (Cornell University Press, Ithaca, 1960), p. 93.
- <sup>24</sup>R. Hultgren, R. D. Desai, D. T. Hawkins, M. Gleiser, and K. K. Kelley, *Selected Values of the Thermodynamic Properties of Binary Alloys* (American Society for Metals, Metals Park, OH, 1973).
- <sup>25</sup>F. Ducastelle, and F. Cyrot-Lackmann, *J. Phys. Chem. Solids* **32**, 285 (1971).
- <sup>26</sup>D. G. Pettifor, *Phys. Rev. Lett.* **42**, 846 (1979).
- <sup>27</sup>R. H. Brown and A. E. Carlsson, *Phys. Rev. B* **32**, 6125 (1985).
- <sup>28</sup>L. R. Mead and N. Papanicolaou, *J. Math. Phys.* **25**, 2404 (1984).
- <sup>29</sup>V. Heine and J. H. Sampson, *J. Phys. F* **13**, 2155 (1983).
- <sup>30</sup>A. R. Miedema, P. F. de Châtel, and F. R. de Boer, *Physica B+C* **100B**, 1 (1980).
- <sup>31</sup>R. E. Watson, L. H. Bennett, and D. A. Goodman, *Acta Metall.* **31**, 1285 (1983).
- <sup>32</sup>R. Hultgren, P. D. Desai, D. T. Hawkins, M. Gleiser, and K. K. Kelley, *Selected Values of the Thermodynamic Properties of the Elements* (American Society for Metals, Metals Park OH, 1973).
- <sup>33</sup>F. Ducastelle and F. Gautier, *J. Phys. F* **6**, 2039 (1976).
- <sup>34</sup>J. B. Cohen, in *Solid State Physics, Advances in Research and Applications*, edited by F. Seitz and D. Turnbull (Academic, New York, 1986), Vol. 39, p. 131.
- <sup>35</sup>This result can be obtained by a high-temperature expansion of the three-body short-range-order parameters, or by the use of a decoupled form for the four-body correlation function analogous to that used in Ref. 14.
- <sup>36</sup>W. Schweika, in *Alloy Phase Stability*, edited by G. M. Stocks and A. Gonis (Kluwer Academic, Boston, 1989), p. 137.
- <sup>37</sup>R. W. Cahn, P. A. Siemers, J. E. Geiger, and P. Bardhan, *Acta Metall.* **35**, 2737 (1987).
- <sup>38</sup>M. K. Phani, J. L. Lebowitz, and M. H. Kalos, *Phys. Rev. B* **21**, 4027 (1980).
- <sup>39</sup>P. Villars and L. D. Calvert, *Pearson's Handbook of Crystallographic Data for Intermetallic Phases* (American Society for Metals, Metals Park, OH, 1985).